Pt Atomically Dispersed in Black TiO 2– x /Cu x O with Chiral-Like Nanostructure for Visible-Light H 2 Generation

Cong Wang, Jingwei Li, Erwan Paineau, Hynd Remita, Mohamed Nawfal Ghazzal

Pt Atomically Dispersed in Black TiO_{2-x}/Cu_xO with chiral like nanostructure for Visible-Light H_2 Generation

Cong Wang,[a] Jingwei Li,[a,c] Erwan Paineau,[b] Hynd Remita[a] and Mohamed Nawfal Ghazzal*[a]

[a]. Institut de Chimie Physique, UMR 8000 CNRS, Université Paris-Saclay 91405 Orsay, France.

[b]. Laboratoire de Physique du Solide, UMR 8502 CNRS, Université Paris-Saclay 91405 Orsay, France.

[c]. School of Chemistry and Chemical Engineering, Institute of Clean Energy and Materials, Guangzhou University 510006 Guangzhou, China.

*Corresponding Author: mohamed-nawfal.ghazzal@universite-paris-saclay.fr

KEYWORDS: black titania, chiral nematic structures, cellulose, single atom, hydrogen evolution.

ABSTRACT: Material design is one of the major driving forces to enhance the intrinsic light harvesting ability of a photocatalyst. Herein, we report the design of black TiO_{2-x}/Cu_xO with chiral-like structures where Pt single atom (SA) are successfully deposited on both black TiO_x and CuO_x for visible-light H_2 generation. Pt are well dispersed in the TiO_x surface but also at the surface of CuO_x, forming single atom alloys (SAAs). Oxygen defects stabilize the SA deposition and Pt SAs significantly enlarge the space charge layer, facilitating both the separation and transfer of photogenerated charge carriers. This structural optimization endows the black TiO_{2-x}/Cu_xO/Pt film excellent light harvesting ability in the visible region, making it a promising visible-light responsive photocatalyst. This work is expected to provide insights into the rational construction of nanostructured materials with chiral nematic structure exhibiting improved light harvesting ability.

1.Introduction

Hydrogen is widely considered as one of the most promising clean energy to realize a decarbonized society.[1] However, the hydrogen currently produced is mostly obtained by reforming methane, an energy-consuming process that emits large amounts of carbon dioxide.[2] To face this so called "grey hydrogen", photocatalytic H_2 generation can realize a direct conversion from solar energy into "green hydrogen", which is beneficial for alleviating the energy crisis and environmental issues.[3]

The photocatalytic efficiency depends on three main key factors, that are, solar light harvesting, photogenerated charge lifetime and surface reactivity.[4] The major driving force to enhance the light harvesting and then the photocatalytic performances is material design. Photonic crystal with periodic dielectric structure provides a unique approach to improve solar light harvesting. The periodic dielectric structure will generate a photonic stop band, where the velocity of photons slows down near the blue and red edges, thereby improving the photochemistry.[5] The confinement of the light in a periodically structured optical medium (due to multiple scattering) enables the control of the light propagation, in particular, can improve the light scattering to enhance the light absorption in films. In this context, cellulose nanocrystals (CNCs), bio-derived material, possess the ability to self-assemble into chiral nematic (Ch) structure, which can be replicated into inorganic materials.[6] Structuring inorganic materials on the mesoscale using a self-biotemplate assembly process appears as a sustainable method for the synthesis of functional materials. For that purpose, impregnation method of free-standing cellulose photonic films, sol-gel self-biotemplating approach and microemulsion were proposed to structure TiO_2 in the films and spheres morphologies for improved photocatalytic hydrogen generation.[7]

Even if these strategies provided an improvement in the photocatalytic efficiency, the activity of nanostructured TiO_2 is still limited to the UV range. To alleviate this restriction, metal nanoparticles are usually used as co-catalysts to promote charge separation by forming an interfacial Schottky barrier.[8] Notably, the size of the nanoparticles can influence markedly the photoactivity of photocatalysts in hydrogen evolution reaction (HER).[9] Downsizing the metallic cocatalyst to the ultimate single atomic site can maximize the atom-utilization efficiency and provide new features that are relevant to construct active interfaces.[10] Single atom (SA) co-catalysts inherit the advantages of heterogeneous and homogeneous catalysts, insuring a high dispersion at the photocatalyst surface and strong-metal support interaction. Moreover, SA exhibit a d-band depletion, which facilitates electronic hybridization and triggers the charge carriers transfer between the photocatalyst and the metal species. One of the major issues facing SAs is their stability against agglomeration. Defects-engineering has been proposed to stabilize SAs. Also, defect-engineering of TiO_2 into black TiO_{2-x} by introducing oxygen vacancy (O_v) is a promising and effective strategy to strengthen light absorption.[11] The defects and low oxidation state in TiO_{2-x} can narrow the bandgap and enable to broaden the spectrum absorption to visible light,[12] but the light harvesting capability remains far from expectation and needs to be further improved. Inspired by this phenomenon, we speculate that the construction of black TiO_{2-x} with chiral nematic like structure coupled with nanoparticles can simultaneously enlarge the absorption range and enhance the light harvesting capability of TiO_2.

Herein, we successfully synthesized black TiO_{2-x}/Cu_xO composite films with Ch nanostructure decorated with Pt SAs. One-pot self-assembly approach was employed to produce TiO_2/Cu_xO films using CNCs as structuring biotemplate.[7a] Subsequently, black TiO_{2-x}/Cu_xO composites were achieved through hydrothermal reduction in the presence of ascorbic acid. The generation of surface oxygen vacancies enables the deposition of Pt SAs, which can enhance the separation of charge carriers. This novel construction showed combined synergetic behaviors: (*i*) the preserved Ch nanostructure pro-

vides enhanced light harvesting capability; (*ii*) oxygen defects enable the broadband absorption under visible light, stabilize the Pt SAs and facilitates electronic hybridization to improve the charge separation. Such unique combination endows the resulting black TiO_{2-x} with chiral nematic like nanostructure with good visible-light H_2 evolution performance.

2. Results

Figure 1a depicts the schematic illustration of fabricating black chiral nematic TiO_{2-x}/Cu_xO films decorated with Pt SAs. The mixture containing CNCs suspension, ethanolic $Ti(acac)_2(OiPr)_2$ and $Cu(OAc)_2$ solution was cast into polystyrene Petri dish. CNCs rods self-organize into helical Ch structures by evaporation induced self-assembly (EISA) process,[7] yielding iridescent $CNC/TiO_2/Cu(OAc)_2$ hybrid film. The Ch structure is evidenced from its fingerprint texture observed under cross-polarized optical microscopy (POM, **Figure 1b and Figure S1**) that corresponds to the helical pitch of the helix (**Figure 1a**).[13] The hybrid films were calcined at 500 ℃ under air to convert the amorphous TiO_2 to anatase, and formed heterojunctions with copper oxides, thus generating freestanding mesoporous TiO_2/Cu_xO films with Ch structures (named Ch-TiO_2/Cu_xO). The Ch structures are well preserved in the inorganic films after the removal of CNCs templates, as evidenced from SEM images showing alternated chiral like multilayers. In addition, the corresponding POM images display strong birefringence where distinctive fingerprint textures are observed (**Figure S2**).

Ascorbic acid was reported as an efficient reductant of TiO_2 to some low-valence-state Ti species (Ti^{3+}), thereby forming defective black TiO_{2-x} forms.[14] In our procedure, Ch-TiO_2/Cu_xO films were impregnated in a 60 mM ascorbic acid aqueous solution and immediately followed by a hydrothermal treatment at 180 ℃ for 24 h. The resulting films turn black (named BCh-TiO_{2-x}/Cu_xO), which attests to the reduction of Ti^{4+} to Ti^{3+} and the creation of O_v.[15] It is worth mentioning that the iridescence of BCh-TiO_{2-x}/Cu_xO films can be observed under natural light as shown in **Figure 1e**, confirming the conservation of the Ch nanostructures. The analysis of the films by POM shows typical fingerprint of the Ch patterns (**Figure S3**), further confirming the preservation of the Ch structure. The BCh-TiO_{2-x}/Cu_xO films are stable under ambient atmosphere, and the O_v-rich surface provides suitable trap sites to stabilize SAs.[16] The Pt SAs decoration was realized by immersing the BCh-TiO_{2-x}/Cu_xO films in 1mM H_2PtCl_6 solution (under anaerobic condition) in the dark for 24 h. The final BCh-TiO_{2-x}/Cu_xO/Pt films displayed the same appearance and structural characteristics as the previous samples (**Figure S4**). Elemental analysis was performed using inductively coupled plasma-optical emission spectrometry (ICP-OES), revealing the mass content of Pt is 0.16 %.

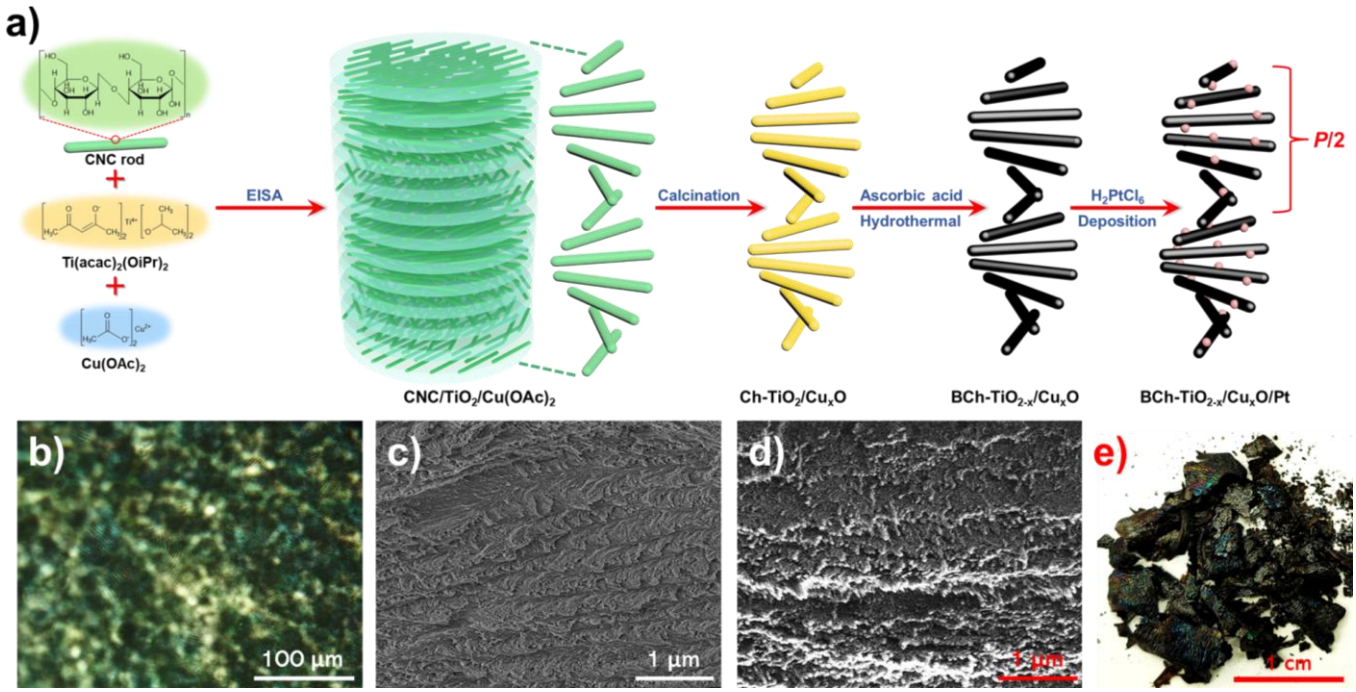

Figure 1. (a) Schematic diagram for the fabrication of BCh-TiO_{2-x}/Cu_xO/Pt films. (b) POM and (c) cross-section SEM images of $CNC/TiO_2/Cu(OAc)_2$. (d) Cross-section SEM image of Ch- TiO_2/Cu_xO. (e) Photograph of BCh-TiO_{2-x}/Cu_xO films showing iridescent colour. There is no change in colour after Pt SAs deposition, and the iridescent colour are still present.

The morphology of the films were revealed by scanning electron microscopy (SEM). The cross-section SEM images of $CNC/TiO_2/Cu(OAc)_2$ film display periodic multilayer with left-handed twist, indicating the formation of Ch structure (**Figure 1c and Figure S5**). Such kind of structure is preserved after the removal of CNCs template by calcination, but with a reduced helical pitch (**Figure 1d, Figure S6a and S6b**). Further hydrothermal treatment and dark deposition only change the visual appearance of the films without affecting the overall Ch nanostructure. Consequently, well-defined multilayers and unique Ch structure remain visible for BCh-TiO_{2-x}/Cu_xO/Pt films (**Figure 2 a-c, Figure S6c and S6d**). To go further, high-resolution transmission electron microscopy (HRTEM) was employed to characterize the nanostructure of BCh-TiO_{2-x}/Cu_xO/Pt films. The interfaces between TiO_2 and Cu_xO are in physical contact to form heterojunctions. The crystal lattices were identified as corresponding to anatase TiO_2 ((101), 3.5 Å) and the mixture of Cu_2O ((200), 2.16 Å)

and CuO ((112), 1.97 Å and (111), 2.35 Å) (**Figure 2d and Figure S7a**).[17] HRTEM further demonstrates that the reduction treatment does not affect the main crystal structure of TiO_2, while introduced amorphous domains in the outer surface region (red dashed lines in **Figure 2d**).[18] The high-angle annular scanning TEM (HAA-STEM) under bright-field and dark-field were performed to confirm the successful Pt SAs anchor. More importantly, HAA-STEM images (**Figure 2d and 2e, Figure S7b**) reveal that Pt atoms exist as individual and isolated species substituted in TiO_2 (101, 3.5 Å), Cu_xO (Cu_2O (211, 1.72 Å) and CuO (111, 2.35 Å)) surface lattice.[19] These observations sustain the formation of single atom alloys (SAA).[20]

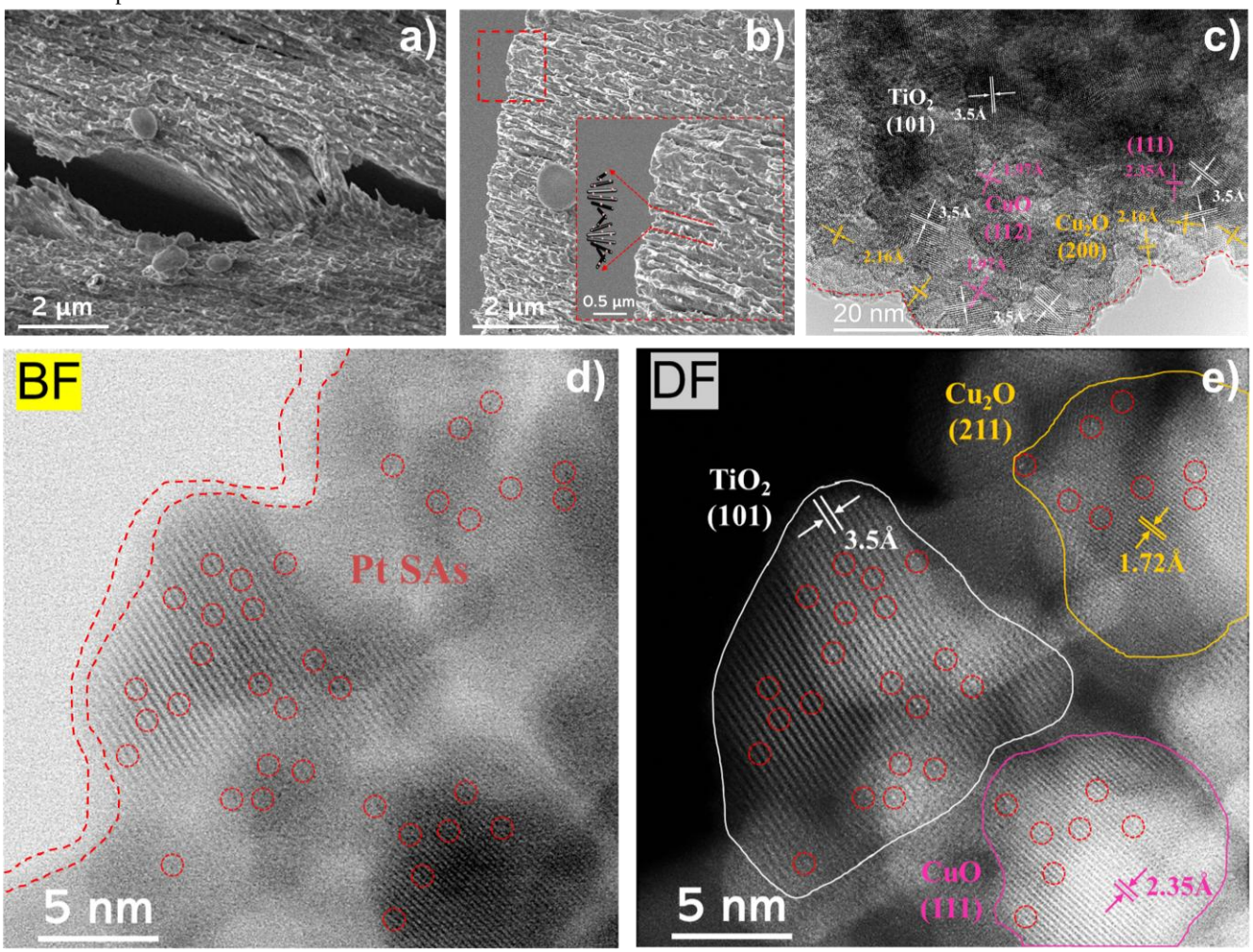

Figure 2. (a, b) SEM images of BCh-TiO_{2-x}/Cu_xO/Pt film observed along the fracture cross-section, showing periodical multilayers. (c) HRTEM image of BCh-TiO_{2-x}/Cu_xO/Pt film. The red dashed line was created to reveal the amorphous region. (d, e) HAA-TEM images of BCh-TiO_{2-x}/Cu_xO/Pt films under bright-field and dark-field showing the distribution of Pt SAs.

The crystalline form of the films was further confirmed by X-ray scattering (XRS). All XRS diagrams are similar and display several well-resolved Bragg reflections related to nanosized TiO_2 crystallites. The indexation of the peaks is in good agreement with the anatase form of TiO_2 (**Figure 3a**). This indicates that the reduction guided by ascorbic acid only occurred on the outer surface of TiO_2 and has no significant effect on bulk crystalline structure.[11b] No diffraction peaks related to Cu or Pt are detected owing to the relatively small particle size and low loading. The UV-vis diffuse reflectance spectra (DRS) was performed to assess the optical properties of composite films (**Figure 3b**). The as-prepared TiO_2 film display typical absorption band of anatase, which is limited to the UV range. The addition of Cu_xO induces a shift of the absorbance to higher wavelength. In comparison, BCh-TiO_{2-x}/Cu_xO exhibits a remarkable broadband absorption covering the entire visible region. The red-shift is attributed to the formation of O_v defects and low-valence-state Ti^{3+}, which are expected to introduce mid-gap states and narrow the bandgap.[11a, 18b] Moreover, the deposition of Pt SAs and formation of SAAs lead to a further enhancement in visible absorption. To confirm that the Ch like structure has an enhancement effect on the light harvesting, we analyzed the absorption spectrum of the films and the same materials, but crushed in a mortar to completely destroy the Ch like structures (**Figure S8a**). Compared to crushed samples, uncrushed samples exhibit enhanced light absorption, especially in the visible rang (**Figure S8b**). This result suggests that Ch like structure play an important role in the enhancement of visible light absorption due to the multiple light scattering. The optical bandgaps were estimated according to Kubelka-Munk (K-M) fitting. As shown in **Figure S9**, the bandgaps of BCh-TiO_{2-x}/Cu_xO and BCh-TiO_{2-x}/Cu_xO/Pt are 1.3 eV and 1.2 eV, respectively, which are smaller than Ch-TiO_2/Cu_xO (2.8 eV). The strong visible absorption and narrow bandgap make BCh-TiO_{2-x}/Cu_xO/Pt films promising photocatalysts under visible

illumination. We performed Raman spectroscopy characterization, whose results are depicted in **Figure 3c, d**. Both pristine TiO_2 and Ch-TiO_2/Cu_xO films present well-resolved peaks. In particular, the characteristic peak at ~ 143 cm^{-1} is shifted compared to BCh-TiO_{2-x}/Cu_xO (≈ 149 cm^{-1}) and BCh-TiO_{2-x}/Cu_xO/Pt (≈ 147 cm^{-1}). This effect originates from the surface reduction of the TiO_2 structure by ascorbic acid, evidencing the reduction of the TiO_2 and the creation of surface defects and O_v.[14a, 21]

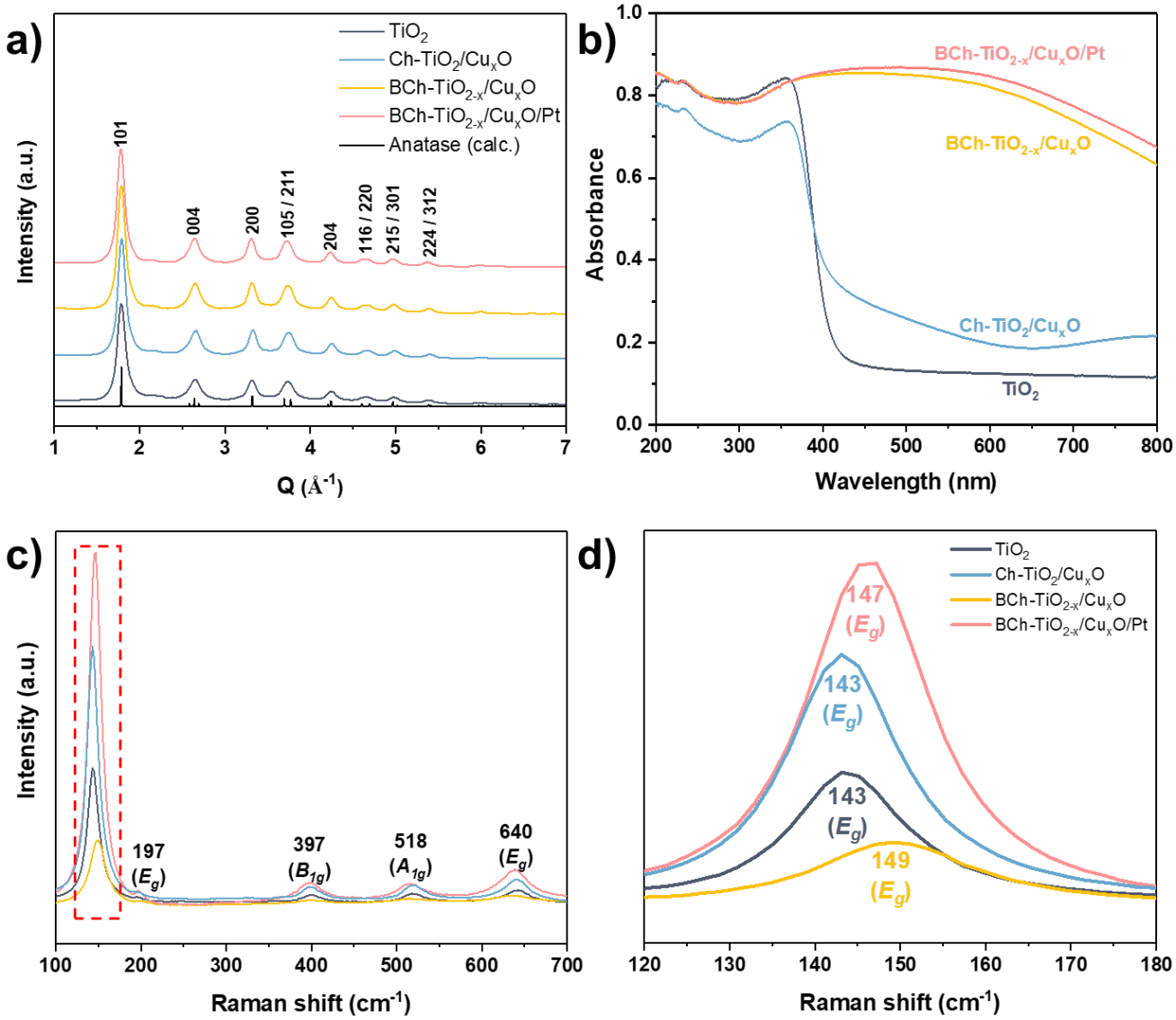

Figure 3. (a) X-ray scattering patterns, (b) UV–vis diffuse reflectance spectra, and (c) Raman spectra of TiO_2, Ch-TiO_2/Cu_xO, BCh-TiO_{2-x}/Cu_xO and BCh-TiO_{2-x}/Cu_xO/Pt composite films. (d) the local enlargement of (c).

X-ray photoelectron spectroscopy (XPS) was employed to further investigate the surface composition of the as-prepared films. The general survey of the films indicates the presence of C, O, Ti, Cu, and Pt species at the surface (**Figure S10**). The Ti 2p shows the typical characteristic peaks for Ti $2p_{3/2}$ and $2p_{1/2}$ at 458.9 eV and 464.6 eV, respectively, corresponding to the Ti^{4+} in TiO_2 (**Figure 4a)**.[22] The Ti 2p spectra are similar for all films, indicating that the bonding environment of Ti atoms is not modified after hydrothermal treatments and deposition of Pt.[11a] The high resolution Cu 2p spectra exhibits two major peaks located at 932.4 eV and 952.3 eV, respectively, which can be attributed to Cu $2p_{3/2}$ and Cu $2p_{1/2}$ (**Figure 4b)**. In terms of the position, these two peaks mainly originate from Cu^+ species, rather than Cu^{2+} species, which usually have higher binding energies.[23] However, the broad satellite peak can be observed in Ch-TiO_2/Cu_xO film, proving the existence of CuO.[24] Notably, the satellite peaks are not detected in black films after hydrothermal reduction using ascorbic acid, which suggests that part of the Cu^{2+} is reduced to Cu/Cu^+ during this process. The O1s XPS spectra of TiO_2 can be deconvoluted into three peaks, i.e., lattice oxygen (O_L, 530.1 eV), surface defects (O_v, 531.6 eV) and adsorbed H_2O (O_{ads}) with higher binding energy (**Figure 4c**).[25] Compared with the pristine TiO_2, black TiO_{2-x} displays a significant increase in the concentration of O_v, which is attributed to the formation of oxygen vacancy and/or surface defects in agreement with the results of UV-Vis and Raman spectroscopies.[18b, 26] Whereas the concentration of O_v decreases again after loading Pt, which is probably due to the coverage of a large amount of O_v by Pt atoms, suggesting the successful

anchoring of Pt SAs.[27] According to the Pt 4f spectrum, Pt^0 and Pt^{2+} are predominantly found in BCh-TiO_{2-x}/Cu_xO/Pt film (**Figure 4d)**. Consistent with previous studies, typical peaks of Pt^{2+}/Pt^0 in Pt SA are located at 76.1/74.2 eV and 72.8/70.9 eV, respectively, corresponding to Pt $4f_{5/2}$ and Pt $4f_{7/2}$.[28] The positively charged Pt SAs are indicative of the existence of strong interactions between the metal and the support materials, allowing the two-way electron transfer to promote the photocatalytic reaction.[29]

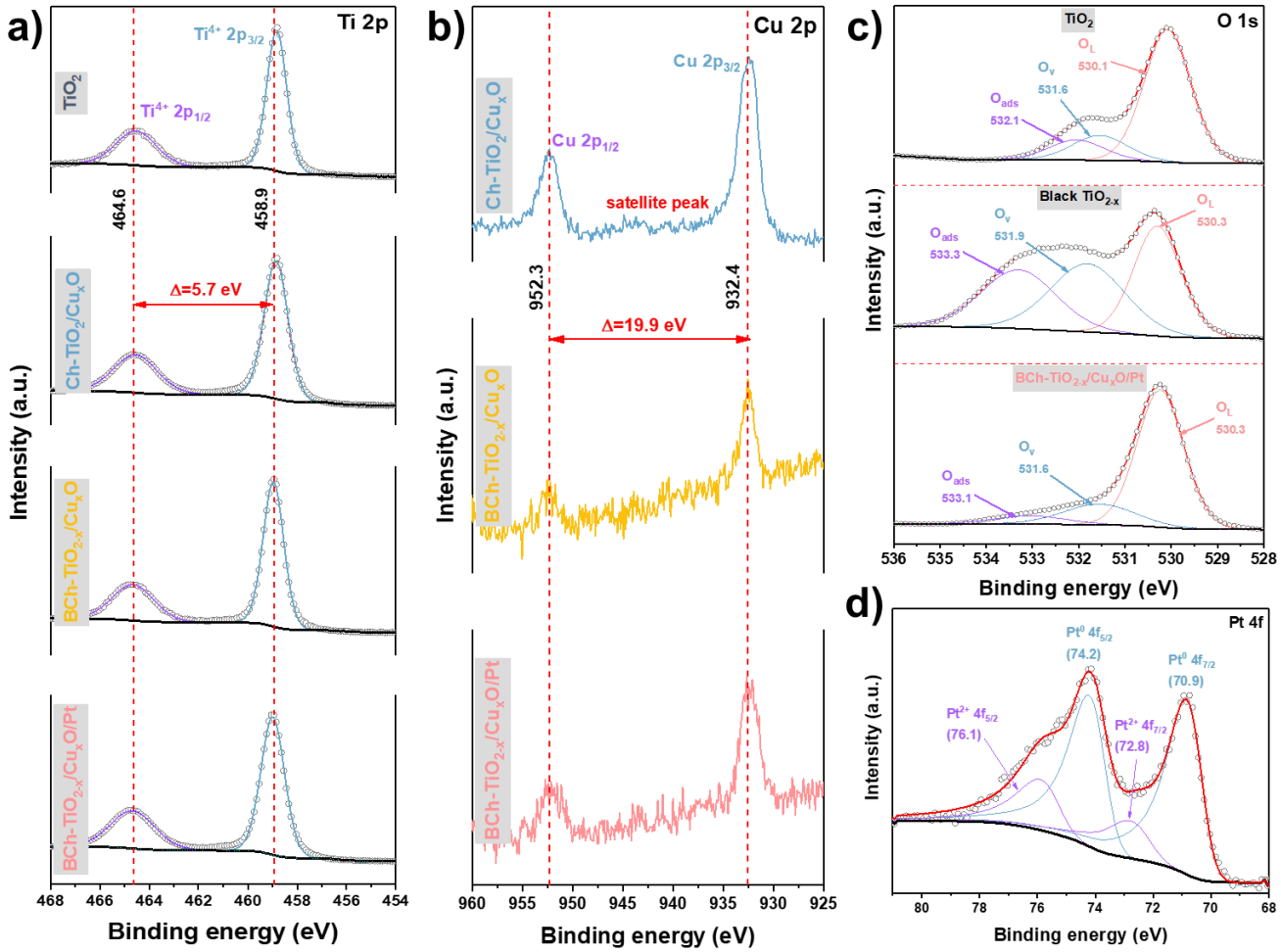

Figure 4. XPS spectra of (a) Ti 2p, (b) Cu 2p, (c) O 1s and (d) Pt 4f corresponding to TiO_2, Ch-TiO_2/Cu_xO, BCh-TiO_{2-x}/Cu_xO and BCh-TiO_{2-x}/Cu_xO/Pt films.

Mott-Schottky (MS) measurement were carried out to reveal the band structures and spatial band bending regions of composites.[30] All MS plots display positive slopes that possess n-type feature. Compared to Ch-TiO_2/Cu_xO, the flat-band potential of TiO_2 shifts from -0.64 to -0.59 eV due to the constructed internal electric fields in bandgap overlapped TiO_2-Cu_xO interfaces with band bending (**Figure 5a**). The introduction of O_v in BCh-TiO_{2-x}/Cu_xO enlarges the spatial charge layer region of internal electric fields on TiO_{2-x}-Cu_xO interfaces, resulting in a positive shift of -0.56 V compared to Ch-TiO_2/Cu_xO.[31] Notably, the deposition of Pt SAs on O_v of BCh-TiO_{2-x}/Cu_xO induces a re-equilibrium of Fermi energy levels on BCh-TiO_{2-x}/Cu_xO/Pt interfaces, which leads obviously to a positive shift to -0.35 V, with respect to BCh-TiO_{2-x}/Cu_xO. This suggests the formation of a significantly enlarged space charge layer, which is beneficial for the transfer and separation of photogenerated charge carriers.[31-32] Electrochemical impedance spectroscopy (EIS) was performed to provide insight into the photogenerated charge carriers transfer capability of composites. The smaller curvature radius on Nyquist plots relates to the lower charge transfer resistance (R_{ct}) at the interfaces of the photocatalyst.[24, 33] A significant reduction of R_{ct} is noticed in BCh-TiO_{2-x}/Cu_xO/Pt films with respect to others, indicating that Pt SAs possess a strong metal-support interaction and play key role in improving charges transfer efficiency, in agreement with the MS plot (**Figure 5b**). In addition, the semicircle radius of all composites further decreases due to the generation of more carriers under light irradiation. The charge separation efficiency and redox ability of composite films are further analyzed by the cyclic voltammetry (CV) curves. In comparison, the BCh-TiO_{2-x}/Cu_xO/Pt exhibits relatively higher redox peak intensity, which relates to the highest redox ability and charge transfer efficiency (**Figure S11**).[34]

The photocatalytic activity of composite films was investigated through HER under visible light excitation (>420 nm). TiO_2 shows rather negligible amount of H_2 generation, while Ch-TiO_{2-x}/Cu_xO develops interesting activity under visible light with kinetic rate of H_2 production of 12.7 $\mu mol \cdot g^{-1} \cdot h^{-1}$. The reduced BCh-$TiO_{2-x}$/$Cu_xO$ films show significantly improved H_2 generation rate of 20.4 $\mu mol \cdot g^{-1} \cdot h^{-1}$ (**Figure 5c and**

Figure S12) in good agreement with the absorption and photoelectrochemical measurements. The decoration of Pt SAs leads to an additional enhancement in photocatalytic activity with an H_2 evolution rate 46 times higher than that of TiO_2 under visible light. No significant photocatalyst deactivation was observed in the HER measurements after four consecutive cycles, indicating the robust stability of BCh-TiO_{2-x}/Cu_xO/Pt (**Figure S13**). Based on the above investigations and characterisations, photocatalytic mechanism over BCh-TiO_{2-x}/Cu_xO/Pt films is proposed as summarized in **Figure S14**. The generated Ti^{3+}-O_v on the TiO_{2-x} surface leads to the formation of valence band (VB) and conduction band (CB) tailing and a consequent bandgap narrowing, which enables the absorption in visible region.[35] Upon visible light irradiation, photogenerated electrons could be excited from the VB of black TiO_{2-x} to its CB and subsequent migrate to Pt SAs deposited on the TiO_x and/or Cu_xO. As demonstrated above, Pt SAs significantly enlarge the space charge layer, facilitating both the transfer and separation of photogenerated charge carriers. As part of the process, Pt SAs and Pt/CuO_x SAAs are suggested to act as reduction sites with prolonged charge carriers lifetime. The O_v surface defects are able to increase the donor density and further participate in improving the charge transfer and reduce the charge carriers recombination.[18b] Moreover, Pt SAs can expand the spatial overlapped region and result in a further enhancement in charge carriers separation. BCh-TiO_{2-x}/Cu_xO/Pt benefits from multireduction sites producing higher H_2 under visible light illumination.

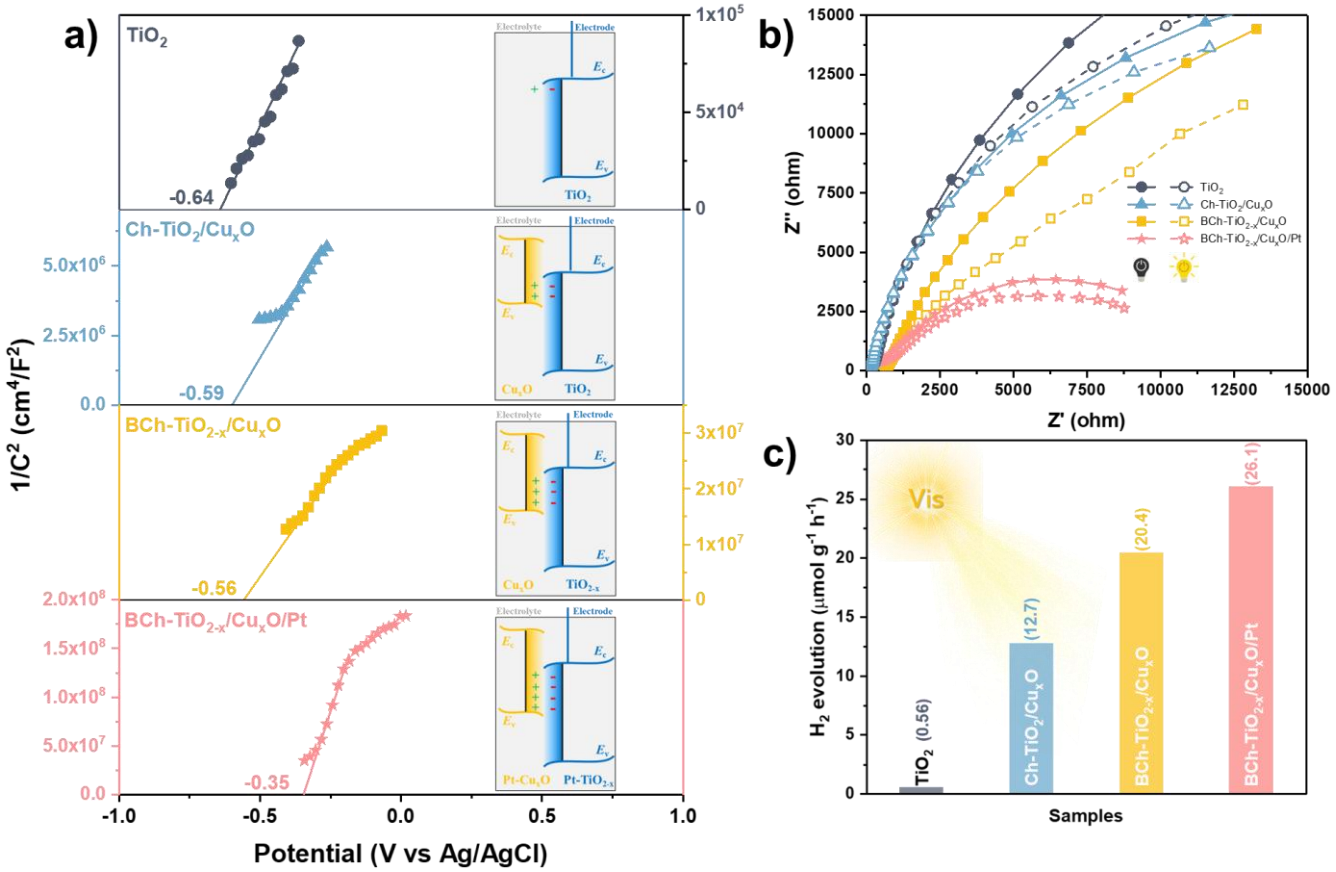

Figure 5. (a) Mott-Schottky plots of TiO_2, Ch-TiO_2/Cu_xO, BCh-TiO_{2-x}/Cu_xO and BCh-TiO_{2-x}/Cu_xO/Pt composite films. Insets are the schematic of band bending. (b) EIS Nyquist plots of composite films under dark (solid line) and light illumination (dotted lines) situations. (c) H_2 evolution rate of composite films under visible light ($\lambda > 420$ nm).

3. Conclusions

In summary, we used cellulose nanocrystals as biotemplates to fabricate a black TiO_{2-x}/Cu_xO/Pt composite film with chiral nematic photonic nanostructure through simple one-pot self-assembly method and hydrothermal reduction. The combination of chiral nematic structure and abundant oxygen vacancies endows the black film with both enhanced light-harvesting capability and broadband absorption in the visible region. In addition, the deposition of Pt single atoms can significantly expand the spatial overlapped region for band bending, favoring the photogenerated charge separation and resulting in an excellent photocatalytic H_2 evolution efficiency under visible light. This unique coupling approach offers a promising strategy to meet the challenges of solar light utilization and charge separation in TiO_2-based photocatalysts.

ASSOCIATED CONTENT

Supporting Information

Synthetic details of BCh-TiO_{2-x}/Cu_xO/Pt; associated characterizations include POM, SEM, HRTEM, XPS; electrochemical and photocatalytic experiments (PDF)

AUTHOR INFORMATION

Corresponding Author

Mohamed Nawfal Ghazzal − Institut de Chimie Physique, UMR 8000 CNRS, Université Paris-Saclay, Orsay 91405, France; orcid.org/0000-0002-2040-995X; Email: mohamed-nawfal.ghazzal@universite-paris-saclay.fr

Authors

Cong Wang − Institut de Chimie Physique, UMR 8000 CNRS, Université Paris-Saclay, Orsay 91405, France ; orcid.org/0000-0002-5071-2562

Jingwei Li − School of Chemistry and Chemical Engineering, Institute of Clean Energy and Materials, Guangzhou University 510006 Guangzhou, China.

Erwan Paineau − Laboratoire de Physique du Solide, UMR 8502 CNRS, Université Paris-Saclay 91405 Orsay, France; orcid.org/0000-0002-6776-7201

Hynd Remita − Institut de Chimie Physique, UMR 8000 CNRS, Université Paris-Saclay, Orsay 91405, France; orcid.org/0000-0003-3698-9327

Present Addresses

Jingwei Li − Institut de Chimie Physique, UMR 8000 CNRS, Université Paris-Saclay, Orsay 91405, France

Author Contributions

M.-N.G. and C.W. conceived the idea. J. W. L. conducted the photo-electro chemistry experiments. E.P. carried out the polarized optical microscopy, Raman spectroscopy and X-ray scattering experiments. C.W. curated the data. H.R. discussed the results. C.W., J. W. L. and M.-N.G. wrote the paper with the help from all authors.

Funding Sources

Cong Wang acknowledges the China Scholarship Council (CSC) for his fellow research position.

Notes

The authors declare no conflict of interest.

ACKNOWLEDGMENT

The authors thank François Brisset for collecting the SEM images, Paul Haghi-Ashtiani for the TEM images and Cyrille Hamon for his assistance in the Raman measurements.

REFERENCES

[1] S. van Renssen, *Nature Climate Change* **2020**, 10, 799.

[2] R. W. Howarth, M. Z. Jacobson, *Energy Science & Engineering* **2021**, 9, 1676.

[3] a) W. Zhang, H. He, H. Li, L. Duan, L. Zu, Y. Zhai, W. Li, L. Wang, H. Fu, D. Zhao, *Advanced Energy Materials* **2020**, 11, 2003303; b) J. Li, X. Gao, L. Zhu, M. N. Ghazzal, J. Zhang, C.-H. Tung, L.-Z. Wu, *Energy & Environmental Science* **2020**, 13, 1326; c) J. Li, X. Han, D. Wang, L. Zhu, M. H. Ha-Thi, T. Pino, J. Arbiol, L. Z. Wu, M. Nawfal Ghazzal, *Angewandte Chemie International Edition* **2022**, 61, e202210242.

[4] J. Schneider, M. Matsuoka, M. Takeuchi, J. Zhang, Y. Horiuchi, M. Anpo, D. W. Bahnemann, *Chem. Rev.* **2014**, 114, 9919.

[5] J. I. L. Chen, G. von Freymann, S. Y. Choi, V. Kitaev, G. A. Ozin, *Adv. Mater.* **2006**, 18, 1915.

[6] a) K. E. Shopsowitz, H. Qi, W. Y. Hamad, M. J. Maclachlan, *Nature* **2010**, 468, 422; b) T.-D. Nguyen, E. Lizundia, M. Niederberger, W. Y. Hamad, M. J. MacLachlan, *Chem. Mater.* **2019**, 31, 2174; c) K. E. Shopsowitz, W. Y. Hamad, M. J. MacLachlan, *Angewandte Chemie International Edition* **2011**, 50, 10991.

[7] a) C. Wang, J. Li, E. Paineau, A. Laachachi, C. Colbeau-Justin, H. Remita, M. N. Ghazzal, *J. Mater. Chem. A* **2020**, 8, 10779; b) G. D. Gesesse, C. Li, E. Paineau, Y. Habibi, H. Remita, C. Colbeau-Justin, M. N. Ghazzal, *Chem. Mater.* **2019**, 31, 4851; c) C. Wang, E. Paineau, H. Remita, M. N. Ghazzal, *Chem. Mater.* **2021**, 33, 6925.

[8] a) Jinhui Yang, Donge Wang, Hongxian Han, C. Li*, *Acc. Chem. Res.* **2013**, 46, 1900; b) G. D. Gesesse, C. Wang, B. K. Chang, S. H. Tai, P. Beaunier, R. Wojcieszak, H. Remita, C. Colbeau-Justin, M. N. Ghazzal, *Nanoscale* **2020**, 12, 7011; c) X. Yuan, C. Wang, D. Dragoe, P. Beaunier, C. Colbeau-Justin, H. Remita, *Appl. Catal. B* **2021**, 281, 119457; d) M. G. Méndez-Medrano, E. Kowalska, A. Lehoux, A. Herissan, B. Ohtani, S. Rau, C. Colbeau-Justin, J. L. Rodríguez-López, H. Remita, *J. Phys. Chem. C* **2016**, 120, 25010; e) L. Liu, A. Corma, *Chem. Rev.* **2018**, 118, 4981.

[9] a) J. Ma, X. Tan, Q. Zhang, Y. Wang, J. Zhang, L. Wang, *ACS Catalysis* **2021**, 11, 3352; b) D. Wang, Z.-P. Liu, W.-M. Yang, *ACS Catalysis* **2018**, 8, 7270; c) X. Li, W. Bi, L. Zhang, S. Tao, W. Chu, Q. Zhang, Y. Luo, C. Wu, Y. Xie, *Adv. Mater.* **2016**, 28, 2427.

[10] a) K. Qi, M. Chhowalla, D. Voiry, *Materials Today* **2020**, 40, 173; b) B. H. Lee, S. Park, M. Kim, A. K. Sinha, S. C. Lee, E. Jung, W. J. Chang, K. S. Lee, J. H. Kim, S. P. Cho, H. Kim, K. T. Nam, T. Hyeon, *Nat. Mater.* **2019**, 18, 620; c) L. Zeng, C. Dai, B. Liu, C. Xue, *J. Mater. Chem. A* **2019**, 7, 24217.

[11] a) Xiaobo Chen, Lei Liu, Peter Y. Yu, S. S. Mao, *Science* **2011**, 331, 746; b) C. Yang, Z. Wang, T. Lin, H. Yin, X. Lu, D. Wan, T. Xu, C. Zheng, J. Lin, F. Huang, X. Xie, M. Jiang, *J. Am. Chem. Soc.* **2013**, 135, 17831; c) Y. Zhao, Y. Zhao, R. Shi, B. Wang, G. I. N. Waterhouse, L. Z. Wu, C. H. Tung, T. Zhang, *Adv. Mater.* **2019**, 31, 1806482.

[12] X. Liu, G. Zhu, X. Wang, X. Yuan, T. Lin, F. Huang, *Advanced Energy Materials* **2016**, 6, 1600452.

[13] J. A. Kelly, M. Yu, W. Y. Hamad, M. J. MacLachlan, *Advanced Optical Materials* **2013**, 1, 295.

[14] a) T. D. Nguyen, J. Li, E. Lizundia, M. Niederberger, W. Y. Hamad, M. J. MacLachlan, *Adv. Funct. Mater.* **2019**, 29, 1904639; b) L. Andronic, A. Enesca, *Frontiers in Chemistry* **2020**, 8, 565489; c) M. Wajid Shah, Y. Zhu, X. Fan, J. Zhao, Y. Li, S. Asim, C. Wang, *Sci Rep* **2015**, 5, 15804.

[15] L. Lu, G. Wang, Z. Xiong, Z. Hu, Y. Liao, J. Wang, J. Li, *Ceram. Int.* **2020**, 46, 10667.

[16] X. Zhou, I. Hwang, O. Tomanec, D. Fehn, A. Mazare, R. Zboril, K. Meyer, P. Schmuki, *Adv. Funct. Mater.* **2021**, 31, 2102843.

[17] a) E. Guo, L. Yin, *Phys. Chem. Chem. Phys.* **2015**, 17, 563; b) Y. Liu, B. Zhang, L. Luo, X. Chen, Z. Wang, E. Wu, D. Su, W. Huang, *Angew. Chem. Int. Ed. Engl.* **2015**, 127, 15475; c) A. Kubiak, Z. Bielan, M. Kubacka, E. Gabała, A. Zgoła-Grześkowiak, M. Janczarek, M.

Zalas, A. Zielińska-Jurek, K. Siwińska-Ciesielczyk, T. Jesionowski, *Appl. Surf. Sci.* **2020**, 520, 146344.

[18] a) J. Kang, Y. Zhang, Z. Chai, X. Qiu, X. Cao, P. Zhang, G. Teobaldi, L. M. Liu, L. Guo, *Adv. Mater.* **2021**, 33, 2100407; b) J. Cai, M. Wu, Y. Wang, H. Zhang, M. Meng, Y. Tian, X. Li, J. Zhang, L. Zheng, J. Gong, *Chem* **2017**, 2, 877; c) W. Zhou, W. Li, J. Q. Wang, Y. Qu, Y. Yang, Y. Xie, K. Zhang, L. Wang, H. Fu, D. Zhao, *J. Am. Chem. Soc.* **2014**, 136, 9280.

[19] A. Sahai, N. Goswami, S. D. Kaushik, S. Tripathi, *Appl. Surf. Sci.* **2016**, 390, 974.

[20] F. R. Lucci, J. Liu, M. D. Marcinkowski, M. Yang, L. F. Allard, M. Flytzani-Stephanopoulos, E. C. Sykes, *Nat. Commun.* **2015**, 6, 1.

[21] W. Hu, W. Zhou, K. Zhang, X. Zhang, L. Wang, B. Jiang, G. Tian, D. Zhao, H. Fu, *J. Mater. Chem. A* **2016**, 4, 7495.

[22] M. N. Ghazzal, H. Kebaili, M. Joseph, D. P. Debecker, P. Eloy, J. De Coninck, E. M. Gaigneaux, *Appl. Catal. B* **2012**, 115-116, 276.

[23] a) P. Jiang, D. Prendergast, F. Borondics, S. Porsgaard, L. Giovanetti, E. Pach, J. Newberg, H. Bluhm, F. Besenbacher, M. Salmeron, *The Journal of chemical physics* **2013**, 138, 024704; b) Y. Wang, Y. Lü, W. Zhan, Z. Xie, Q. Kuang, L. Zheng, *J. Mater. Chem. A* **2015**, 3, 12796.

[24] M. Z. Hussain, B. van der Linden, Z. Yang, Q. Jia, H. Chang, R. A. Fischer, F. Kapteijn, Y. Zhu, Y. Xia, *J. Mater. Chem. A* **2021**, 9, 4103.

[25] a) A. Naldoni, M. Allieta, S. Santangelo, M. Marelli, F. Fabbri, S. Cappelli, C. L. Bianchi, R. Psaro, V. Dal Santo, *J. Am. Chem. Soc.* **2012**, 134, 7600; b) T. K. Rahul, M. Mohan, N. Sandhyarani, *ACS Sustainable Chemistry & Engineering* **2018**, 6, 3049; c) C. Jia, H.-S. Chen, P. Yang, *Journal of industrial and engineering chemistry* **2018**, 58, 278.

[26] A. Sinhamahapatra, J.-P. Jeon, J.-S. Yu, *Energy & Environmental Science* **2015**, 8, 3539.

[27] X. Hu, J. Song, J. Luo, H. Zhang, Z. Sun, C. Li, S. Zheng, Q. Liu, *Journal of Energy Chemistry* **2021**, 62, 1.

[28] a) Huabin Zhang, Pengfei An, Wei Zhou, Bu Yuan Guan, Peng Zhang, Juncai Dong, X. W. D. Lou*, *Sci. Adv.* **2018**, 4, eaao6657; b) Lei Nie, Donghai Mei, Haifeng Xiong, Bo Peng, Zhibo Ren, Xavier Isidro Pereira Hernandez, Andrew DeLaRiva, Meng Wang, Mark H. Engelhard, Libor Kovarik, Abhaya K. Datye, Y. Wang, *Science* **2017**, 358, 1419; c) John Jones, Haifeng Xiong, Andrew T. DeLaRiva, Eric J. Peterson, Hien Pham, Sivakumar R. Challa, Gongshin Qi, Se Oh, Michelle H. Wiebenga, Xavier Isidro Pereira Hernández, Yong Wang, A. K. Datye, *Science* **2016**, 353, 150.

[29] a) Z. Zeng, Y. Su, X. Quan, W. Choi, G. Zhang, N. Liu, B. Kim, S. Chen, H. Yu, S. Zhang, *Nano Energy* **2020**, 69; b) Y. Chen, S. Ji, W. Sun, W. Chen, J. Dong, J. Wen, J. Zhang, Z. Li, L. Zheng, C. Chen, Q. Peng, D. Wang, Y. Li, *J. Am. Chem. Soc.* **2018**, 140, 7407; c) B. Qiao, A. Wang, X. Yang, L. F. Allard, Z. Jiang, Y. Cui, J. Liu, J. Li, T. Zhang, *Nat. Chem.* **2011**, 3, 634.

[30] J. Li, X. Yang, C. Ma, Y. Lei, Z. Cheng, Z. Rui, *Appl. Catal. B* **2021**, 291, 120053.

[31] I. A. Digdaya, G. W. P. Adhyaksa, B. J. Trzesniewski, E. C. Garnett, W. A. Smith, *Nat. Commun.* **2017**, 8, 15968.

[32] J. Li, J. Chen, H. Fang, X. Guo, Z. Rui, *Ind. Eng. Chem. Res.* **2021**, 60, 8420.

[33] a) D. Ma, Z. Wang, J.-W. Shi, Y. Zou, Y. Lv, X. Ji, Z. Li, Y. Cheng, L. Wang, *J. Mater. Chem. A* **2020**, 8, 11031; b) C. Xu, P. Cao, N. Wang, H. Ma, M. Lin, *Chem. Commun.* **2021**, 57, 8596.

[34] Z. Khazaee, A. R. Mahjoub, A. H. Cheshme Khavar, *Appl. Catal. B* **2021**, 297, 120480.

[35] A. Naldoni, M. Altomare, G. Zoppellaro, N. Liu, S. Kment, R. Zboril, P. Schmuki, *ACS catalysis* **2019**, 9, 345.

Table of Contents

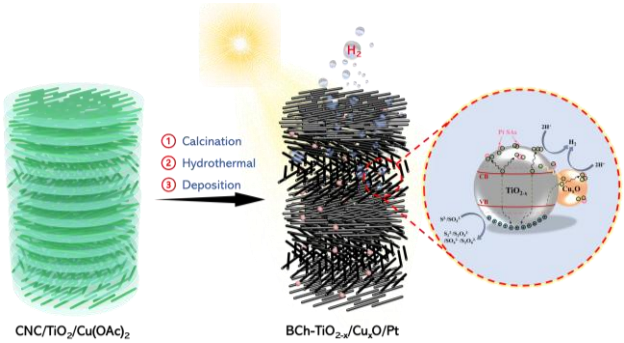
H2
1 Calcination
2 Hydrothermal
3 Deposition
CNC/TiO2/Cu(OAc)2
BCh-TiO2-x/CuxO/Pt